Turkish Journal of Electrical Engineering & Computer Sciences

http://journals.tubitak.gov.tr/elektrik/

Research Article

Turk J Elec Eng & Comp Sci
(2022) 30: 644 – 658
© TÜBİTAK
doi:10.3906/elk-2104-54

# Critical speed calculation of a refurbishment of 11MW hydro power plant unit

**Ahmet Selim PEHLİVAN**[1,*], **Dario KRALJEVIC**[2], **Ivan TRIPLAT**[2], **Beste BAHÇECİ**[3]
[1]TÜBİTAK Marmara Research Center, Energy Institute, Kocaeli, 41470, Turkey
[2]KONCAR GIM, Zagreb, 10000, Croatia
[3]Sabancı University, İstanbul, 34956, Turkey

**Received:** 07.04.2021 • **Accepted/Published Online:** 03.09.2021 • **Final Version:** 21.03.2022

**Abstract:** Hydro generator design is a significant issue in terms of safety, efficiency, and energy production sustainability. One of the most crucial issues about design criteria is to satisfy the needs of the project's critical speed. In this work, the critical speed calculation of an 11 MW hydro power plant was investigated with several design steps. Numerical solution methodologies were implemented using ARMD™. A generator design was developed, and the implementation of the rotor was carried out in Antalya, Turkey. Vibration and displacements of the hydro generator are adequate. The generator unit is active for 3 years and have never encountered runaway speeds. No critical speed or resonance speed is anticipated for the designed hydro generator unit.

**Key words:** Hydro unit rotor, FEM, critical speed, resonance, rotor dynamics

## 1. Introduction

Large hydro turbine generator sets can balance power instantaneously at peak hours and off-hours, thus having the ability to stabilize network frequency and perform phase angle compensation [1]. This stabilization and compensation ability renders them crucial in power networks [2, 3]. With increasing power demands, the replacement of these generator sets poses a unique design challenge with limitations imposed by prior installations [4]. In this study, we consider replacing one such hydro turbine unit, built in Kepez (Antalya, Turkey), as one of the three turbines of the Kepez-1 hydroelectric power plant. The power plant initially provided 16 MW of power in 1958, which was upgraded to 8.8 MW per generator unit, which is 26.4 MW total, with the increase in energy demand. Recently, under the MILHES Project, a new update was initiated for the Kepez-1 power plant. The project aims to increase the efficiency of the hydroelectric power plant using national resources in the design stage and the manufacturing process of new units. Accordingly, a vertical type of Francis turbine, a synchronous generator, a speed regulator, an excitation system, and a SCADA system were designed, manufactured, and used in the Kepez-1 power plant.

Controlling vibration is a crucial factor in the safety and stability considerations in designing a new turbine [5–7]. Excessive vibration in the shaft of the hydro turbine generator unit could lead to malfunctions of the system components, ultimately leading to reduced safety [8–10]. Shaft vibrations are categorized as axial, torsional, and lateral [11]. Lateral vibration is influenced by guide-bearing stiffness, the distance of bearings, stiffness of the shaft, the mass of rotor, system's rotational speed, magnetic pull, hydraulic force, mechanical force, and the eccentricity of unit shaft system [11–13]. A lateral vibration model could be used in understanding

*Correspondence: spehlivan@sabanciuniv.edu



This work is licensed under a Creative Commons Attribution 4.0 International License.

oscillation phenomena within the mechanism, in failure diagnosis, and the condition-based maintenance of the power plant units [14]. However, the vibration response analysis of a hydro turbine generator unit is almost an intractable problem due to complicated boundary conditions, external excitations, hydraulic forces, and magnetic pull [11]. These boundary conditions are complicated due to the guide-bearing oil film forces dependent on rotational speed and eccentricity [11]. In addition to that, external excitations are caused by mechanical forces, which are also dependent on rotational speed [11]. In the literature, a variety of methods are introduced to calculate the vibration response. Most of these methods include periodic excitation forces but not random excitation forces [14–18]. Finite element methods (FEM) and transfer matrix methods (TMM) are standard methods of modeling a shaft system [19–21]. Throughout this work, we employ FEM in our modeling and vibrational analysis of the shaft system of the replacement turbine unit due to its greater accuracy compared to TMM [5].

The theoretical runaway speed of a turbine is the limit of a large hydroelectric power plant's running speed. The previously installed turbine in the Kepez-1 power plant had a nominal speed of 750 rpm and a runaway speed of 1360 rpm. As new design criteria, runaway speed was aimed at 1430 rpm with a 1.9 ratio to nominal speed, and an even higher critical speed of a sizeable inertial rotor was stipulated for the recently designed work. Average running speeds can be selected to have a higher ratio; however, submergence needs to be deeper during operation to avoid cavitation. The main challenge in this particular mode of operation is to design a high-speed hydro turbine generator with an increased runaway speed that must fit into the existing space from the previous generator unit with a lower runaway speed, as the new unit must replace the previous one. In the following sections, the design steps of the hydro turbine generator unit with the stipulations discussed above will be detailed, and lateral vibration simulations in ARMD™ will be presented.

## 2. Methodology

The critical speed of a simple shaft can be determined analytically. When a shaft is in stationary condition distance between the geometric center and center of mass is called $e$ (eccentricity present of the shaft), the mass of the shaft is $m$, the distance between the geometric center and end of the shaft is $d$, and spring constant of upper and lower bearings of the shaft are $k_u$ and $k_l$, respectively (Figure 1a). When the shaft is in rotating condition, deflection occurs on the shaft due to angular velocity. Angular velocity is called $w$, deflection due to rotation is called $y$ (Figure 1b).

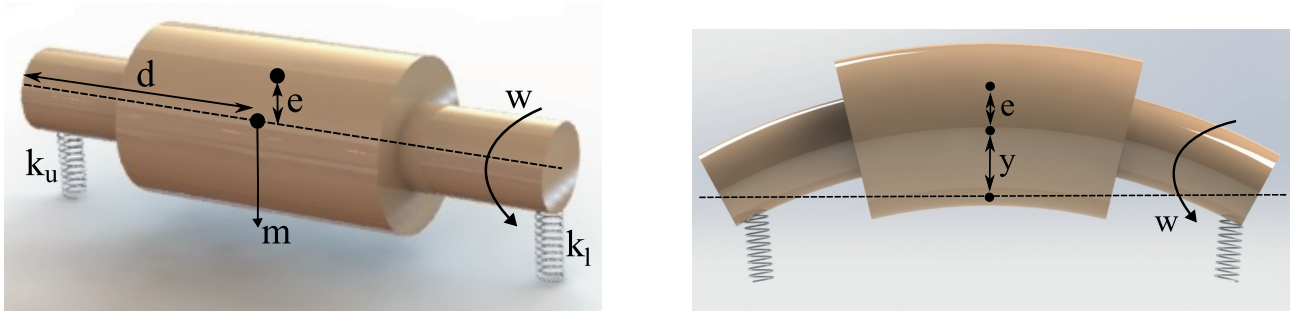


(a) Shaft in stationary condition

(b) Shaft in rotating condition

**Figure 1**. Shaft in stationary and rotating conditions.

In Equation 1, $F_c$ is centrifugal force, in Equation 2, $F_r$ is restoring force, $K$ is stiffness of the shaft in lateral direction. When the shaft is in rotating condition, centrifugal force should be equal to restoring force of the shaft for the equilibrium of the system Equation 3. While rearranging Equation 3, Equation 4 and can be calculated.

$$F_c = m \times w^2 \times (y + e). \tag{1}$$

.

$$F_r = K \times y. \tag{2}$$

$$m \times w^2 \times y + m \times w^2 \times e = K \times y. \tag{3}$$

$$y = \frac{m \times w^2 \times e}{K + m \times w^2} = \frac{\frac{w^2 \times e}{K/m}}{1 - \frac{w^2}{K/m}}. \tag{4}$$

The natural frequency of a system is the frequency where the system vibrates with a maximum amplitude which means the resonance condition of the system. For this simple shaft system value of angular frequency ($W_n$) which makes deflection ($y$) maximum is $\sqrt{\frac{K}{m}}$ Equation 5. Combining Equations **??** and 5, Equation 6 can be established.

$$W_n = \sqrt{\frac{K}{m}}. \tag{5}$$

$$y = \frac{\frac{w^2 \times e}{W_n^2}}{1 - \frac{w^2}{W_n^2}}. \tag{6}$$

The stiffness of the shaft is computed as in Equation 7, where $W$ is the weight of the shaft, $\xi$ is the static deflection of the shaft due to weight, and $g$ is the gravitational acceleration. Static deflection of a simply supported beam where the load is at the center of the beam is given in Equation 8. $l$ is the length of the beam, $E$ is Young's modulus, and $I$ is inertia. The inertia of a simply supported beam can be evaluated as in Equation 9, where $d$ is the radius of the beam.

$$K = \sqrt{\frac{W}{\frac{\xi}{m}}} = \sqrt{\frac{m \times g}{\xi \times m}} = \sqrt{\frac{g}{\xi}}. \tag{7}$$

$$\xi = \frac{W \times l^3}{48 \times E \times I}. \tag{8}$$

$$I = \frac{\pi}{64} \times d^4. \tag{9}$$

## 3. Simulation results and discussion

The rotor of the replacement unit consists of the turbine runner and the rotor of the generator. The generator rotor has two guide bearings: the upper guide bearing, which is located above the rotor poles, and the lower guide bearing, below the generator (Figure 2a). The third radial bearing is on the turbine side. The upper and lower guide bearings are center-pivoted, tilting-pad bearings. The upper bearing has four guide pads. On

the other hand, the lower guide bearing has two guide pads at the same time. The turbine guide bearing is a circular bearing that has two arcs. The thrust bearing is also a center pivoted, tilting pad bearing with twelve pads. All three bearings on the unit's rotor are used to damp the dynamic effects, the calculation of which includes the stiffness and damping coefficients of the oil film between the bearing pads and the rotor shafts.

The analysis was done for lateral and torsional critical speed since those loadings are dominant in operation due to rotational behavior. For lateral vibrations, two cases were considered, with and without the influence of magnetic field. The nominal speed for the observed geometry of the turbine–generator unit was 750 rpm, while the theoretical runaway speed was 1430 rpm. According to design requirements for lateral vibrations, the first critical speed of the turbine–generator unit had to be at least 20% greater than theoretical runaway speed, for the turbine used in this work, it must be greater than 1716 rpm. Moreover, according to design requirements for torsional vibrations, the first critical speed had to be safely removed from exciting frequencies, including the nominal speed of 750 rpm, the theoretical runaway speed of 1430 rpm, twice the nominal speed of 1500 rpm, and the grid frequency of 50 Hz. Critical speed analysis was performed using the ARMD V5.7 application from RBTS Inc. The software is based on finite element method using Euler–Bernoulli-based beam elements for shaft discretization. In other words, vibration analysis was performed using a linear material model. The material used in the analysis was AISI 4140 alloy steel with material properties relevant to linear theory given by $E = 210000N/mm^2$ (Young's modulus), $= 0.3$ (Poisson's ratio), and $G = 80769N/mm^2$, (Shear modulus) and all electrical systems are chosen to be copper. Bearing characteristics are calculated with the help of hydrodynamic analysis, stiffness and damping values are calculated for 750 rpm, 1430 rpm, and 1630 rpm speeds, that are nominal speed, theoretical runaway speed, and estimated first critical speed of the generator.

There were three main stages in the design process. In order to achieve the project's design requirements, three significant attempts were completed with finite element model simulations. In the initial design attempt, the length of the shaft was larger than 4 m due to different physical design necessities, such as the upper bracket design was not converged and longer than the final one. The distance between the bearings was 3810 mm.

At this design stage, the result of rotor dynamics was investigated with simulations. Results showed that the design requirements were not achieved with this initial design. In the second design stage, the distance between bearings was aimed to diminish with some consecutive design changes on the stator frame and upper bearing. The distance between bearings was reduced to 3440 mm. With this design attempt, the requirement for critical speed, which needs to be around 1710 rpm, was not achieved. In the final stage of design changes, the main aim was achieved by reducing the bearing distance to 2481 mm with substantial design changes. Shortening the length of the rotor also necessitates design changes on the stator frame and brackets. At this design stage, numerical calculations for rotor dynamics were also conducted, and sufficient critical speed was achieved.

### 3.1. First design attempt

Radial stiffness and damping components, which were calculated with spring constants of lower and upper guide bearings and brackets, applied as boundary conditions to upper and lower guide bearings.

In Figure 2b, the model used for lateral vibration analysis is presented in 2D. This model includes two generator bearings (upper bearing – UGB and lower bearing – LGB) and one turbine bearing (TB). Discs represented additional masses (generator rotor and turbine runner). The generator rotor has a mass of 30,700 kg, and the turbine runner has a mass of 1410 kg.

Since fluid film bearings used in the system are flexible, their dynamic characteristics are defined using

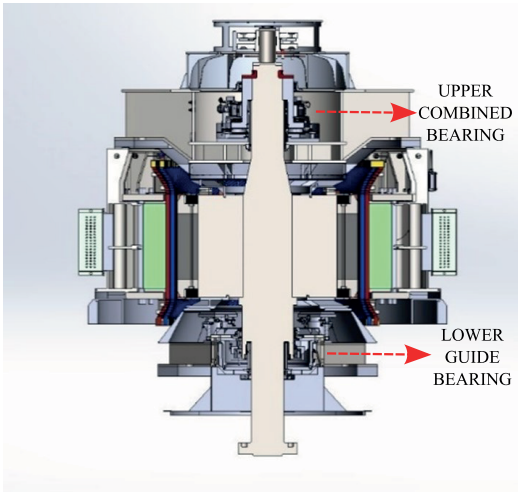


(a) Generator cross section.

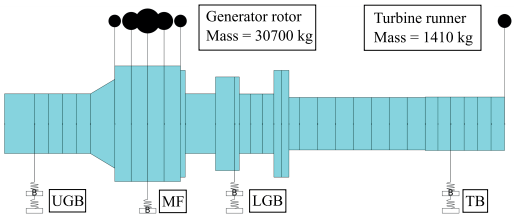


(b) Model used for lateral critical speed calculation on first design attempt..

**Figure 2**. Generator cross section and model used for lateral critical speed calculation.

stiffness coefficient $k[N/m]$ and damping coefficient $c[Ns/m]$ in the two perpendicular radial directions for planar motion (horizontal and vertical). The supplying companies provided the values of stiffness and damping matrices which were 2 by 2 matrices. Stiffness and damping values depend primarily on the bearing design and shaft speed of rotation such as the nominal speed. The influence of the magnetic field was modeled similarly as with the modeling of the bearings employing stiffness. However, the values of the stiffness matrix must be negative since the magnetic field creates additional electromagnetic force perpendicular to the shaft, which influences the value of lateral vibrations such as the critical speed. The value of the stiffness due to the magnetic field was 0.086 MN/mm. Besides, the contribution of the generator bearing support structure was considered by defining stiffness matrices for each bearing housings (UGB, LGB, and TB) and the overall mass of the bearing support structure in two perpendicular directions (Figure 3a). Unbalanced vibrations result from an unbalanced force or unbalanced moment. An unbalanced force arises from the eccentricity of the mass center of the rotating parts, while an unbalanced moment arises when the rotating part (disc) is not mounted perpendicular to the axis of rotation of the shaft. Since unbalanced vibrations are something that cannot be neglected, this is also included when defining analysis parameters by defining unbalance as in ((10)).

$$U = m \times e. \tag{10}$$

Where m is the mass of the rotor, and e is the eccentricity that defines the real mass center. Another factor with a significant influence on the critical speed is the gyroscopic effect, which was also considered by defining moments of inertia for rotating parts represented as discs in the numerical model. The model involves an assumption that the shaft is rotationally symmetric. With all these factors included and modeled at the software ARMD, lateral critical speed analysis results without the influence of magnetic field are presented in Figure 3a and Table 1.

Figure 3a and Table 1 show that the first lateral critical speed is 948 rpm with an undetermined direction of precession, while the second is 1063 rpm with forward precession, meaning that the direction of rotation of the orbit (elliptical curve) due to eccentricity is the same as the direction of shaft rotation. If we have a situation

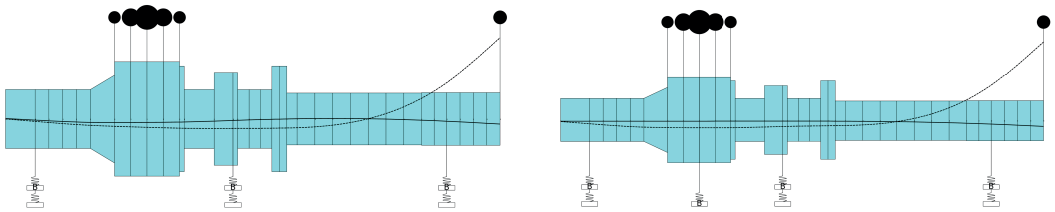

(a) First lateral mode without magnetic field ( $n_0$ = 948 rpm, $\xi$ = 0 .3141 )

(b) First lateral mode with magnetic field ( $n_0$ = 811 rpm, $\xi$ = 0 .231 )

**Figure 3**. First lateral mode with and without magnetic field.

**Table 1**. Lateral critical speed calculation results without magnetic field.

| | Critical speed (rpm) | Damping value ($\xi$) |
|---|---|---|
| First lateral mode | 948 | 0.3141 |
| Second lateral mode | 1063 | 0.308 |
| Third lateral mode | 1594 | 0.457 |

with counter rotations, that would be a backward or reverse precession, meaning that the solution to the eigenvalue problem such that the natural frequency is negative. Since 750 rpm is not in the vicinity of the first lateral critical speed, an unbalanced response analysis was performed. With the aim of running the unbalance analysis, dynamic properties for all previously mentioned factors such as unbalanced magnetic field and bearing stiffnesses influencing the critical speed had to be defined for three speed values. For the initial speed value, a nominal speed of 750 rpm was chosen; similarly, the intermediate and final speed values 1430 rpm and 1650 rpm were assigned, with several speed increments set to 50. Unbalanced response analysis calculates vibratory amplitudes and phases at all locations along the shaft for a defined range of rotational speeds, presented in Figure 7a for the positions where the bearings are located (UGB, LGB, and TB). Unbalanced response solution indicates that critical speed occurs around 1130 rpm, the value at which the vibration amplitude is maximum that was taken as the final value for the case without the influence of the magnetic field.

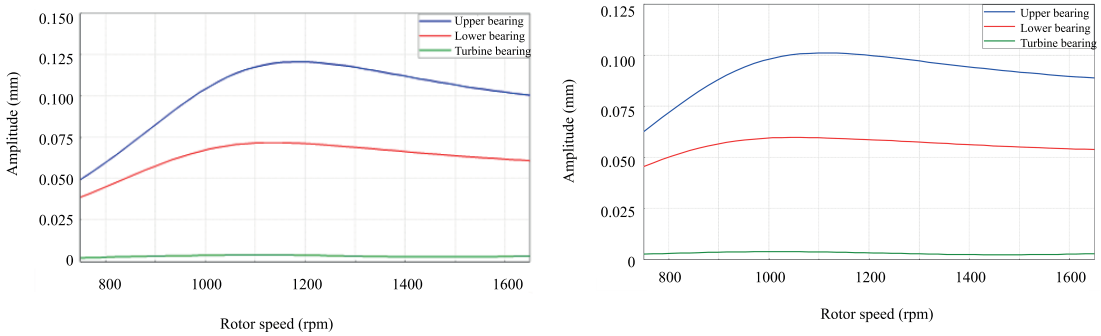


(a) Response without magnetic field ( $n_0$ = 1130 rpm). rpm).

(b) Response with magnetic field ( $n_0$ = 1050 rpm). rpm).

**Figure 4**. Response with and without magnetic field.

Lateral critical speed analysis results for the case with the influence of magnetic field are presented in

**Table 2**. Lateral critical speed calculation results with magnetic field.

| | Critical speed (rpm) | Damping value ($\xi$) |
|---|---|---|
| First lateral mode | 811 | 0.231 |
| Second lateral mode | 902 | 0.229 |
| Third lateral mode | 1617 | 0.440 |

Figure 3b and Table 2. The first lateral critical speed is 811 rpm with forward precession. This critical speed refers to the case without the influence of the magnetic field. Since 750 rpm is again not close to the first lateral critical speed, response analysis was performed for the same range of speeds. Unbalanced response analysis results for the case with magnetic field are presented in Figure 7b for the bearings' three positions. Unbalanced response solution indicates that critical speed occurs around 1050 rpm, the value at which the vibration amplitude is maximum which was taken as the final value for the case with the influence of the magnetic field.

The same model for lateral vibrations was used for torsional vibration analysis. However, for this type of vibration analysis, not all the factors mentioned above affect the value of critical torsional speed for instance the natural frequency, since this type of analysis is one order lower than the lateral vibrations. Hence, fewer input files are required for the definition of the model. In general, the polar moment of inertia for rotating parts and material properties alongside the geometry of the turbine is not necessary for computation. The generator unit is all the requirement. Torsional critical speed analysis results are presented in Figures 5a and 5b.

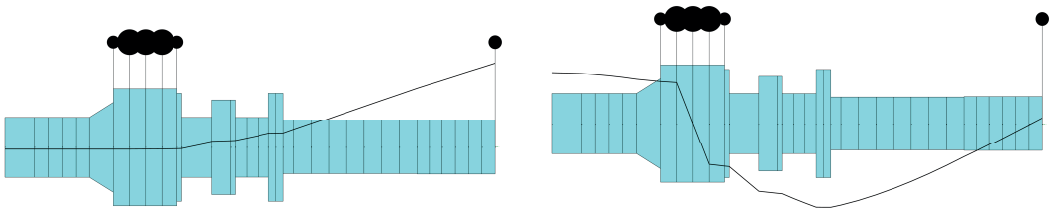

(a) First torsional mode ( $n_0$ = 2286 rpm) (b) Second torsional mode ( $n_0$ = 11277 rpm).

**Figure 5**. First and second torsional modes.

### 3.2. Second design attempt

In the second design attempt, an increase of a factor of two in the upper bearing UGB oil film stiffness was proposed, for which an increase of 100 rpm in the first lateral critical speed was predicted. Additionally, a 100 rpm increase in the first lateral critical speed was predicted. Second design model for lateral vibration analysis was obtained after shortening the shaft length by about 400 mm, reducing the shaft diameter in the rotor position from 650 to 500 mm, moving lower bearing LGB position for around 150 mm up and applying various other updates, alongside changing the stiffness of generator bearing support structure (Figure 6).

The overall mass of all rotating parts in second model is 28,680 kg instead of 34,280 kg in first model, thus leading to a mass reduction of around 16%. Lateral critical speed analysis results with the changes mentioned above included and modeled. Simulation models without the influence of the magnetic field are presented in Figure 7a and Table 3.

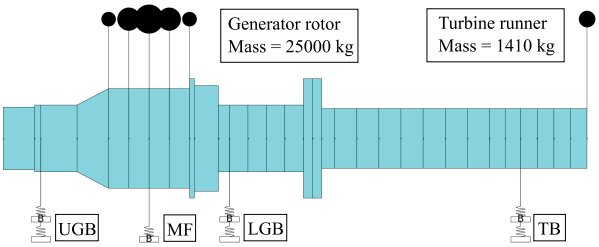


**Figure 6**. Model used for lateral critical speed calculation on second design attempt.

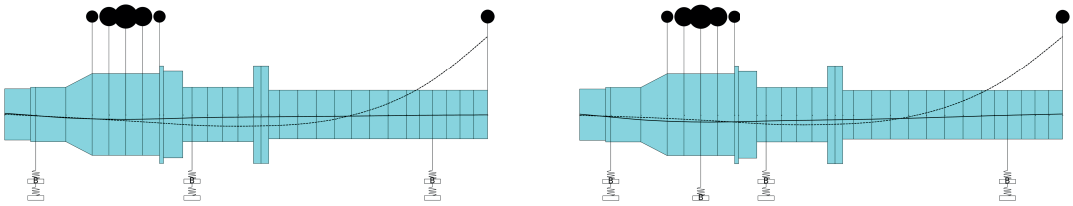

(a) First lateral mode without magnetic field ( $n_0$ = 1163 rpm, $\xi$ = 0 .434).

(b) First lateral mode with magnetic field ( $n_0$ = 975 rpm, $\xi$ = 0 .508).

**Figure 7**. First lateral mode with and without magnetic field.

**Table 3**. Lateral critical speed calculation results without magnetic field.

| | Critical speed (rpm) | Damping value ($\xi$) |
|---|---|---|
| First lateral mode | 1163 | 0.434 |
| Second lateral mode | 1423 | 0.418 |
| Third lateral mode | 1577 | 0.437 |

As seen in Figure 7a, the first lateral critical speed is at 1163 rpm with forward precession, which is higher than in the first design attempt. Since 750 rpm is again not in the vicinity of the first lateral critical speed, unbalanced response analysis was performed. Dynamic properties for all factors influencing critical speed were selected for three speeds: A nominal speed of 750 rpm for the initial speed, 1430 rpm for the medium speed, and 2500 rpm for the final speed, with the number of speed increments equal to 50, same as in the previous stage. Unbalanced response analysis results for the case without magnetic field are presented in Figure 8a for the bearing locations. Unbalanced response solution indicated that critical speed occurs around 1600 rpm, the value at which the vibration amplitude is maximum, taken as the final value for the case without the influence of the magnetic field.

Lateral critical speed analysis results for the case with the influence of magnetic field for second design attempt geometry of turbine and generator unit are presented in Figure 7b and Table 4.

As seen in Figure 7b and Table 4, the first lateral critical speed is 975 rpm with an undetermined direction of precession, which is lower than the case with no influence of the magnetic field but more extensive than the critical speed found in the first design step. Unbalanced response analysis was performed since 975 rpm is far from the first lateral critical speed which is 750 rpm. Results of the analysis for the case with magnetic field are presented in Figure 8b for different positions of the bearings. The critical speed value obtained from this analysis, i.e. the speed at which the vibration amplitude is maximum (1520 rpm), was taken as the final value

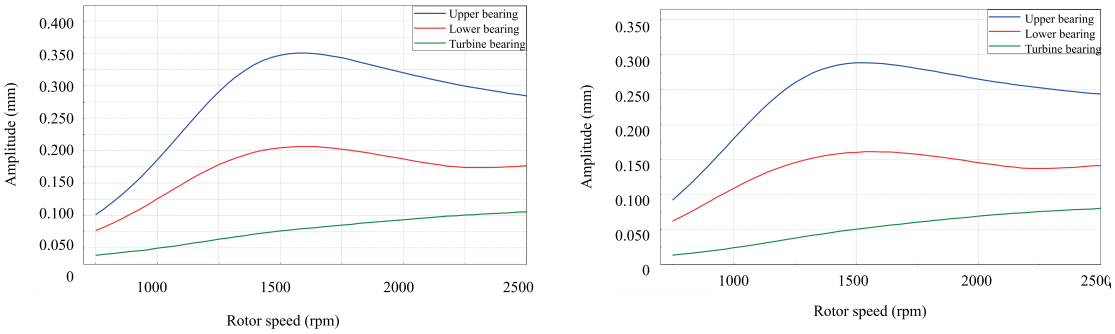


(a) Unbalanced response without magnetic field ( $n_0$ = 1600 rpm).

(b) Unbalanced response with magnetic field ( $n_0$ = 1520 rpm).

**Figure 8**. Unbalanced response with and without magnetic field.

**Table 4**. Lateral critical speed calculation results with magnetic field.

| | Critical speed (rpm) | Damping value ($\xi$) |
|---|---|---|
| First lateral mode | 975 | 0.508 |
| Second lateral mode | 1265 | 0.481 |
| Third lateral mode | 1576 | 0.436 |

for the case with the influence of the magnetic field.

Torsional critical speed analysis results for applied geometry and stiffness changes on turbine–generator unit are presented in Figures 9a and 9b.

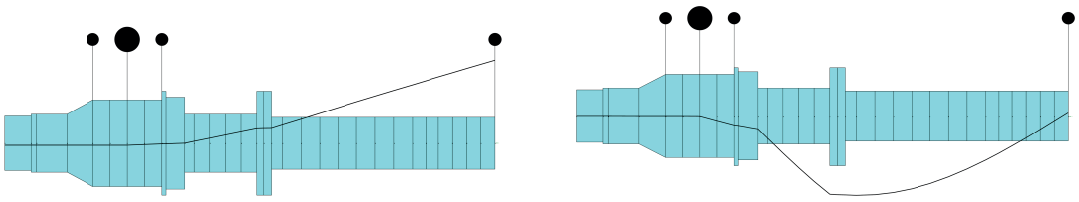

(a) First torsional mode ( $n_0$ = 2305 rpm)

(b) Second torsional mode ( $n_0$ = 15242 rpm).

**Figure 9**. First and second torsional modes.

Based on the calculations presented for critical lateral speeds, it was concluded that the first critical speed occurs at 1520 rpm and that the value is again below the requirement which was 1716 rpm. However, considering that the first critical speed for this second design step is above the load rejection speed as opposed to that of the first design step and 12% above the theoretical runaway speed, the conclusion was that the generator should work accurately. Based on the calculations presented for critical torsional speeds, it was concluded that the first critical speed occurs around 2305 rpm and is safely separated from the exciting frequencies of the highest value of 1500 rpm.

### 3.3. Final design attempt

Considering that the value of lateral critical speed still was not satisfying the exact design criteria, alterations are made on the turbine generator model. The length of the shaft is shortened by approximately 20 mm. The diameter of the shaft flange is increased from 600 to 700 mm. The UGB position is moved up by approximately 10 mm, and the LGB position is moved approximately 7 mm down. After various other updates, such as changing the stiffness of generator bearing support structure at the upper and lower bearing positions, the final design step model for lateral vibration analysis was obtained and is presented in Figure 10.

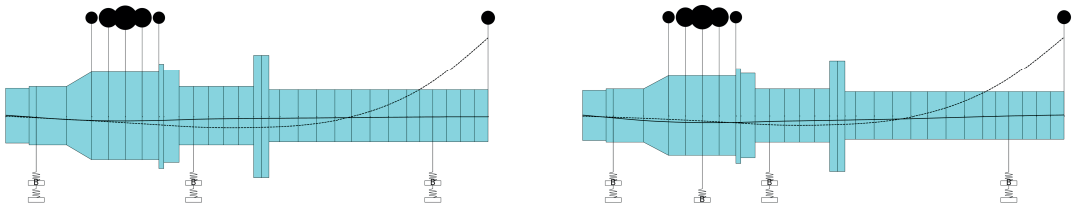

(a) First lateral mode without magnetic field ($n_0$ = 1157 rpm, $\xi$ = 0.434).

(b) First lateral mode with magnetic field ($n_0$ = 967 rpm, $\xi$ = 0.509).

**Figure 10**. Model used for lateral critical speed calculation on final design attempt.

The overall mass of all rotating parts in the final design stage is 28,780 kg instead of 28,680 kg, which is the mass in second design stage, which resulted from dimension changes. With all the changes included and modeled, the lateral critical speed analysis results without the influence of magnetic field are presented in Figure 11a and Table 5.

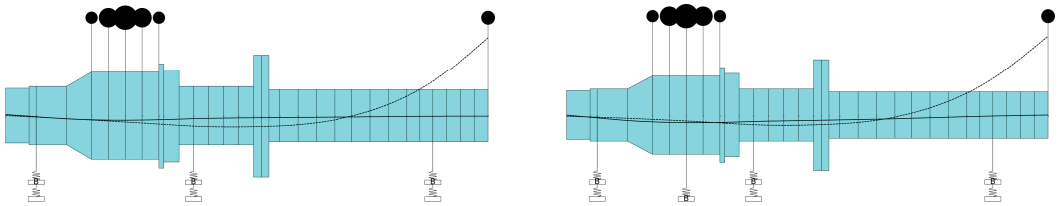

(a) First lateral mode without magnetic field ($n_0$ = 1157 rpm, $\xi$ = 0.434).

(b) First lateral mode with magnetic field ($n_0$ = 967 rpm, $\xi$ = 0.509).

**Figure 11**. First lateral mode with and without magnetic field.

**Table 5**. Lateral critical speed calculation results without magnetic field.

| | Critical speed (rpm) | Damping value ($\xi$) |
|---|---|---|
| First lateral mode | 1157 | 0.434 |
| Second lateral mode | 1409 | 0.420 |
| Third lateral mode | 1574 | 0.433 |

As shown in Figure 11a, the first lateral critical speed is 1157 rpm with forward whirl, which is higher than in the first design phase but lower than in the second design phase. Response analysis was performed to find the value for the lateral critical speed. Dynamic properties for all factors influencing the critical speed were defined within the same speed range as in the previous stage. Response analysis results for the case without

magnetic field are presented in Figure 12a for positions where bearings are located as Figure 11a. Response solution points out that critical speed occurs around 1570 rpm, the value at which the vibration amplitude is maximum which was taken as the final value for the case without the influence of the magnetic field.

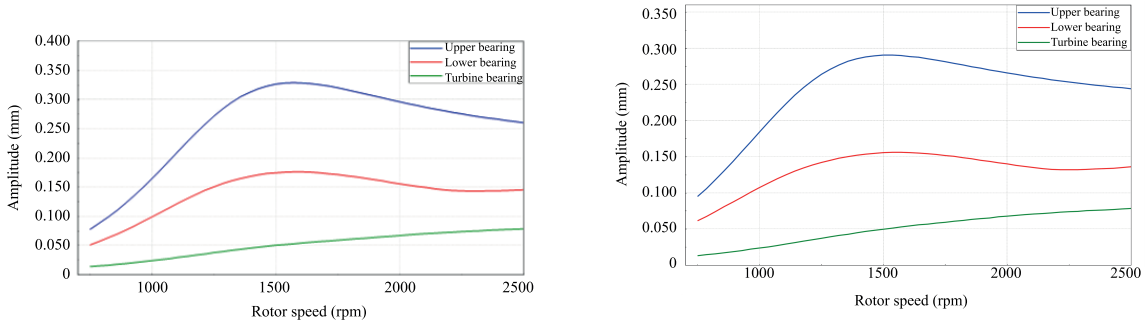


(a) Response without magnetic field ( $n_0$ = 1570 rpm)

(b) Response with magnetic field ( $n_0$ = 1500 rpm)

**Figure 12**. Response with and without magnetic field.

Lateral critical speed analysis results for the case with the influence of magnetic field for final stage turbine and generator unit are presented in Figure 11b and Table 6. The first lateral critical speed is 967 rpm with an undetermined direction of precession and is lower than the one in the case without the influence of the magnetic field. The first lateral critical speed is also slightly lower than that of the second design phase but again higher than that of the first design stage. Response analysis was performed to find the value for lateral critical speed. This analysis for the case with the magnetic field is presented in Figure 12b for various positions of bearings. Response solution indicates that critical speed occurs at approximately 1500 rpm, the value at which the vibration amplitude is maximum which was taken as the final value for the case with the influence of the magnetic field.

**Table 6**. Lateral critical speed calculation results with magnetic field.

| | Critical speed (rpm) | Damping value ($\xi$) |
|---|---|---|
| First lateral mode | 967 | 0.509 |
| Second lateral mode | 1259 | 0.484 |
| Third lateral mode | 1573 | 0.433 |

Torsional critical speed analysis results for applied geometry and stiffness changes on turbine and generator unit in the final design phase are presented in Figure 13a and 13b. Based on the calculations presented for critical lateral speeds, it was calculated that the first critical speed occurs around 1570 rpm and that the value is below design criteria which were 1716 rpm. Considering that the first critical speed for this design attempt, as opposed to first design attempt, is above load rejection speed and is 10% above the theoretical runaway speed, the conclusion was made that the generator should work accurately. Based on the calculations presented for critical torsional speeds, it is concluded that the first critical speed occurs around 2294 rpm and is safely separated from exciting frequencies whose highest value is 1500 rpm.

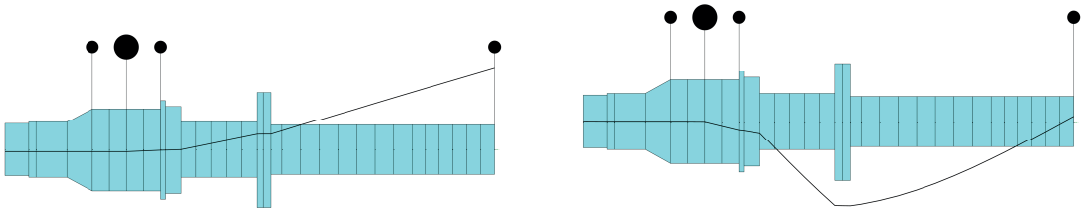

(a) First torsional mode ( $n_0$ = 2294 rpm) (b) Second torsional mode ( $n_0$ = 12240 rpm).

**Figure 13**. First and second torsional modes.

## 4. Implementation results and discussion

In this section, implementation results will be presented. The new hydro generator unit designed and implemented at Kepez with active power of the 9.3 MW (see Figure 14a), previous unit had an active power of 8.8 MW. Nominal speed of working rotor can be seen in Figure 14b as 750 RPM.

In Figures 15a to 16a, bearing displacements of the rotor is presented. In Figures 15a, x-axis and y-axis displacement of upper guide bearing is shown. x-axis displacement is around 65 µm and y-axis displacement is around 80 µm. Lower guide bearing displacement data is given in Figures 15b. x- axis displacement is around 110 µm and y-axis displacement is around 105 µm. In Figure 16a, turbine bearing displacement is presented, x-axis average displacement of turbine bearing is settled to 55 µm and average y-axis displacement is settled to 43 µm.

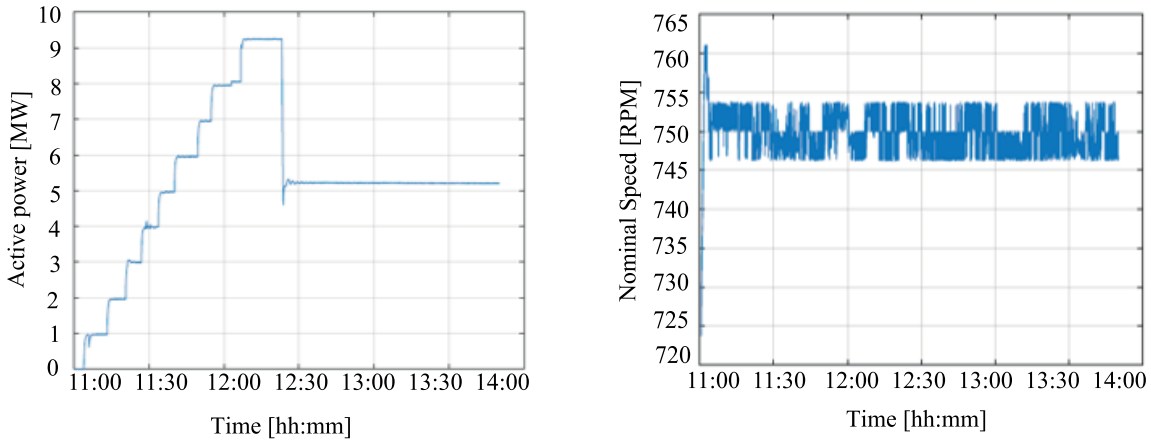


(a) Active power graph of the rotor. (b) Nominal speed data of the rotor.

**Figure 14**. Results of hydro power plant.

Bearing vibration data is given in Figure 16b. Upper guide bearing vibration is represented by blue line in the figure and it changes between 0.3 and 0.2 $mm/s^2$. Lower guide vibration is presented by red line and it changes between 0.2 and 0.1 $mm/s^2$. Finally, green line presents turbine bearing vibration, and it changes between 0.3 and 0.1 $mm/s^2$.

As has been shown in figures, vibration and displacements of the unit are much lower than the desired values. The unit is under operation and had never encountered of runaway speeds. No critical speed or resonance speed are expected for the new designed unit.

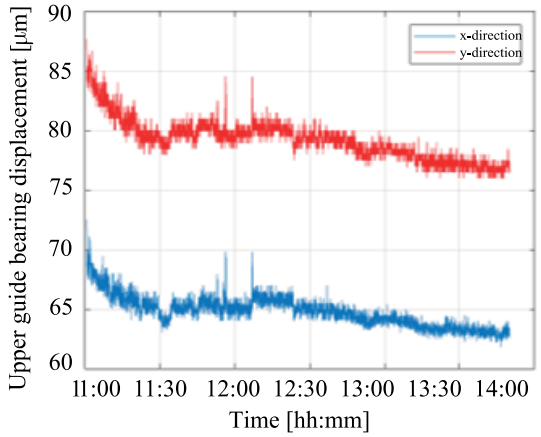


(a) Upper guide bearing displacement.

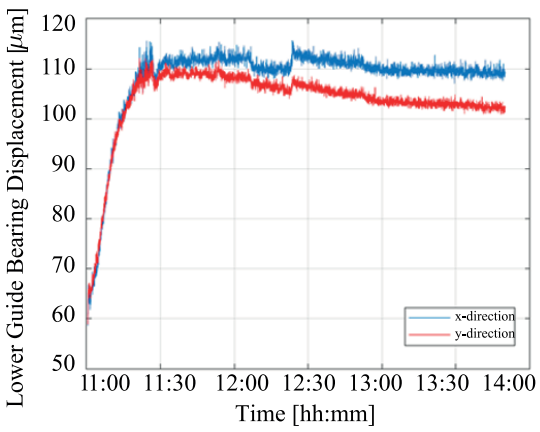


(b) Lower guide bearing displacement.

**Figure 15**. Results of hydro power plant.

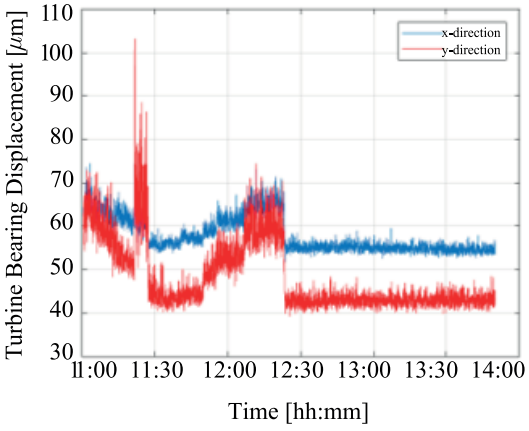


(a) Turbine bearing displacement (blue line is x-axis displacement, red line is y-axis displacement).

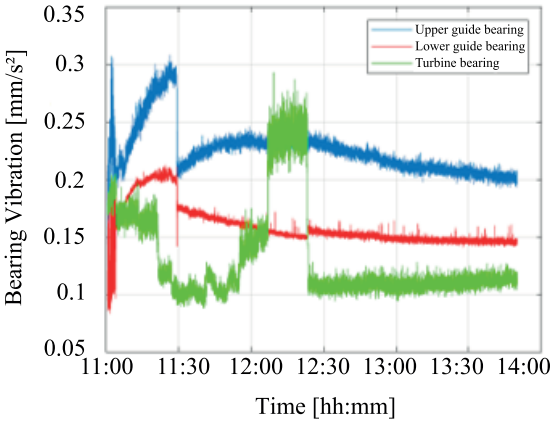


(b) Bearing vibration graph for upper guide bearing (blue), lower guide bearing (red) and turbine bearing (green).

**Figure 16**. Results of hydro-power plant.

## 5. Conclusion

In numerical calculations, the first designed system discussed above is failing to meet design specifications. The distance between the shaft and the bearings in the first designed system is 3810 mm (see Figure 17a). This number was chosen due to the practicality of assembly and placement. However, critical speed specifications cannot be met with this design.

Distance between bearings is one of the issues that contribute to the bearing instability problem since the distance between supporting points is directly proportional to the stiffness of the rotor system. Bearing distance reduction leads to a stiffer and more robust rotor design, which meets the design requirements. A new design is produced with a shorter distance between lower and upper guide bearings. As shown in Figure 17b, in the latest design, the distance is 2450 mm. Reducing the distance between guide bearings changes every design parameter. For this reason, all static parts that hold rotor and bearings must be and were redesigned.

In addition to decreasing the distance between bearings, the bearings' oil was changed from ISO VG 68 to ISO VG 46. The oil film damping and stiffness changes due to the viscosity of the oil type, and VG 46 possesses a larger spring constant of dynamic oil film than VG 68. The change in oil type was thus implemented to increase the oil film damping and stiffness. These alterations resulted in reaching critical speed specifications.

After design criteria was met, the hydro generator design was completed, and the implementation of the rotor was carried out. As has been shown in figures, vibration and displacements of the unit are much lower than the desired values. The unit is under operation and had never encountered runaway speeds. Vibration and displacement data of the implemented hydro unit indicate that the design is effective, and critical speed or resonance speed is not expected for the designed generator unit.

In terms of safety against resonance, the newly refurbished generator has a more secure design while the critical speed of the generator was designed 10% higher than the previous generator whereas the volume of the rotor was decreased. Therefore, economically more efficient manufacturing was accomplished. Moreover, the generator's efficiency has improved from 95% to 98.5%. In addition, the possibility of resonance situation has been significantly decreased which leads to longer lifespan for the generator.

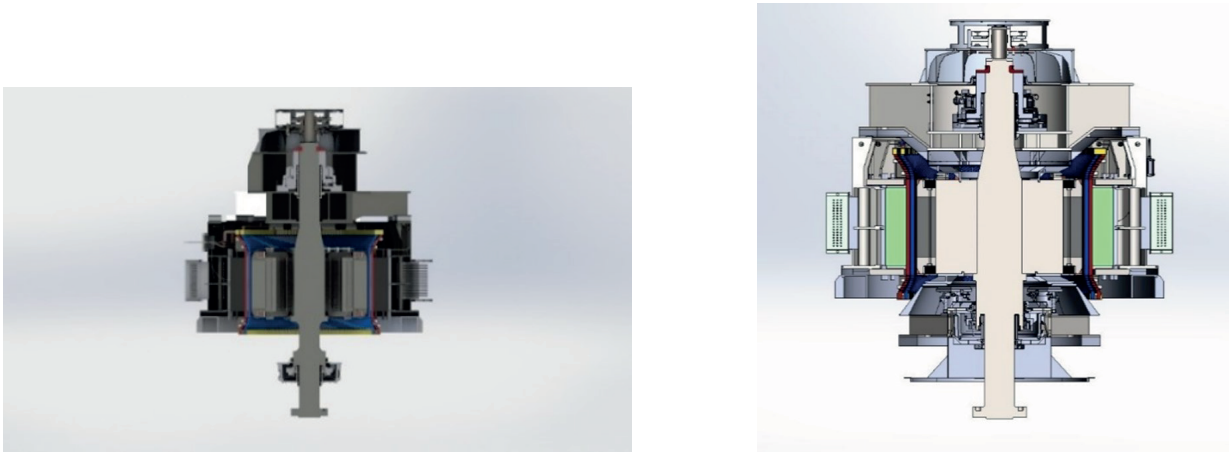

(a) Initial design phase with longer bearing distance

(b) Final design phase with shorter bearing design.

**Figure 17**. Initial and final turbine designs.

**Acknowledgment**

This project was supported by Sabancı University, İstanbul, Turkey by the tuition waiver of Ahmet Selim Pehlivan and Beste Bahçeci.

## References

[1] Beires P, Vasconcelos MH, Moreira CL, Lopes JAP. Stability of autonomous power systems with reversible hydro power plants: a study case for large scale renewables integration. Electric Power Systems Research 2018; 158: 1–14. doi:10.1016/j.epsr.2017.12.028

[2] Nicolet C, Kawkabani B, Greiveldinger B, Herou J, Allenbach P et al. Turbine speed governor parameters validation in islanded production. In: International Meeting of the Workgroup on Cavitation and Dynamic Problems in Hydraulic Machinery and Systems; Timisoara, Romania; 2007.

[3] Platero CA, Sánchez JA, Nicolet C, Allenbach P. Hydropower plants frequency regulation depending on upper reservoir water level. Energies 2019; 12 (9): 1637. doi: 10.3390/en12091637

[4] Altay A, Şahin C, İskender İ, Gezer D, Çakır CA. Compensator design for the aged hydro electric power plant speed governors. Electric Power Systems Research 2016; 133: 257–268. doi:10.1016/j.epsr.2015.12.016

[5] Zeng Y, Zhang L, Guo Y, Qian J, Zhang C. The generalized hamiltonian model for the shafting transient analysis of the hydro turbine generating sets. Nonlinear Dynamics 2014; 76 (4): 1921–1933. doi:10.1007/s11071-014-1257-9

[6] Gustavsson R. Modelling and analysis of hydropower generator rotors. Licentiate dissertation, Luleå University of Technology,Luleå, Switzerland; 2005.

[7] Dollon Q, Monette C, Gagnon M, Tahan A, Antoni J. Calibration of critical speed predictions using experimental measurements. In: IOP Conference Series: Earth Environmental Science; Lausanne, Switzerland; 2021. doi: 10.1088/1755-1315/774/1/012130

[8] Mohanta RK, Chelliah TR, Allamsetty S, Akula A, Ghosh R. Sources of vibration and their treatment in hydro power stations - a review. Engineering Science and Technology, an International Journal 2017; 20 (2): 637–648. doi:10.1016/j.jestch.2016.11.004

[9] Liu D, Ding SC, Wang Z, Yu LJ. Transient response and critical speed analysis of large vertical volute pump. In: IOP Conference Series: Earth Environmental Science; Beijing, China; 2018. doi: 10.1088/1755-1315/163/1/012048

[10] Bai B, Zhang L, Guo T, Liu C. Analysis of dynamic characteristics of the main shaft system in a hydro-turbine based on ANSYS. In: International Conference on Advances in Computational Modeling and Simulation; Kunming, China; 2012. pp. 654-658. doi: 10.1016/j.proeng.2012.01.1081

[11] Bettig BP, Han RPS. Modeling the lateral vibration of hydraulic turbine-generator rotors. Journal of Vibration and Acoustics 1999; 121 (3): 322–327. doi:10.1115/1.2893983

[12] Zou CP, Hua HX, Chen DS. Modal synthesis method of lateral vibration analysis for rotor-bearing system. Computers & Structures 2002; 80 (32): 2537–2549. doi:10.1016/S0045-7949(02)00294-8

[13] Husnjak O, Oreskovic O, Letal J, Kaica F. Identification of hydro unit stiffness, critical speed and vibrating masses based on vibration measurements. Spokane, WA, USA: HydroVision, 2018.

[14] Xu Y, Li Z, Lai X. Dynamic model for hydro-turbine generator units based on a database method for guide bearings. Shock and Vibration 2013; 20: 411–421. doi:10.1155/2013/426849

[15] Feng F, Chu F. Dynamic analysis of a hydraulic turbine unit. Mechanics Based Design of Structures and Machines 2001; 29: 505–531. doi:10.1081/SME-100107625

[16] Xu Y, Li Z, Lai X. Simulation model of radial vibration for a large hydro-turbine generator unit and its application. In: IEEE Power Engineering and Automation Conference; Wuhan, China; 2011. pp 191–195. doi:10.1109/PEAM.2011.6135043

[17] Lai X, Liao G, Zhu Y, Zhang X, Gou Q et al. Lateral vibration of hydro turbine-generator rotor with varying stiffness of guide bearings. IOP Conference Series: Earth and Environmental Science 2012; 15 (2): 1-13. doi:10.1088/1755-1315/15/4/042006

[18] Bucur DM, Cosoiu CI, Iovanel RG, Nicolae AA, Georgescu SC. Assessing the operation of the cooling water system of a hydro-power plant using EPANET. Energy Procedia 2017; 112: 51–57. doi:10.1016/j.egypro.2017.03.1058

[19] Subbiah R, Kumar AS, Sankar TS. Transient dynamic analysis of rotors using the combined methodologies of finite elements and transfer matrix. Journal of Applied Mechanics 1988; 55 (2): 448–452. doi:10.1115/1.3173697

[20] Bai B, Zhang LX, Zhao L. Influences of the guide bearing stiffness on the critical speed of rotation in the main shaft system. In: IOP Conf. Ser.: Earth Environ. Sci. 2012; 15: 1-6. doi: 10.1088/1755-1315/15/7/072028

[21] Jagannath K. Evaluation of critical speed of generator rotor with external load. International Journal of Engineering Research and Development 2012; 11 (1): 11-16.